Biosensors and Bioelectronics 180 (2021) 113109

Contents lists available at ScienceDirect

Biosensors and Bioelectronics

journal homepage: http://www.elsevier.com/locate/bios

Enantioselective SERS sensing of pseudoephedrine in blood plasma biomatrix by hierarchical mesoporous Au films coated with a homochiral MOF

Olga Guselnikova [a,b,*], Hyunsoo Lim [c,d], Jongbeom Na [c], Miharu Eguchi [c,e], Hyun-Jong Kim [f], Roman Elashnikov [a], Pavel Postnikov [a,b], Vaclav Svorcik [a], Oleg Semyonov [b], Elena Miliutina [a,b], Oleksiy Lyutakov [a,b], Yusuke Yamauchi [c,e,**]

[a] Department of Solid State Engineering, University of Chemistry and Technology, 16628, Prague, Czech Republic
[b] Research School of Chemistry and Applied Biomedical Sciences, Tomsk Polytechnic University, 634049, Tomsk, Russian Federation
[c] Australian Institute for Bioengineering and Nanotechnology (AIBN), The University of Queensland, Brisbane, QLD, 4072, Australia
[d] New & Renewable Energy Research Center, Korea Electronics Technology Institute (KETI), 25, Saenari-ro, Bundang-gu, Seongnam-si, Gyeonggi-do, 13509, Republic of Korea
[e] JST-ERATO Yamauchi Materials Space-Tectonics Project and International Center for Materials Nanoarchitectonics (WPI-MANA), National Institute for Materials Science (NIMS), 1-1 Namiki, Tsukuba, Ibaraki, 305-0044, Japan
[f] Surface Technology Group, Korea Institute of Industrial Technology (KITECH), Incheon, 21999, Republic of Korea

ARTICLE INFO

Keywords:
Mesoporous gold
Homochiral MOF
SERS
Pseudoephedrine
Biosensor
Blood plasma

ABSTRACT

Here, we present a new family of hierarchical porous hybrid materials as an innovative tool for ultrasensitive and selective sensing of enantiomeric drugs in complex biosamples *via* chiral surface-enhanced Raman spectroscopy (SERS). Hierarchical porous hybrid films were prepared by the combination of mesoporous plasmonic Au films and microporous homochiral metal-organic frameworks (HMOFs). The proposed hierarchical porous substrates enable extremely low limit of detection values (10^{-12} M) for pseudoephedrine in undiluted blood plasma due to dual enhancement mechanisms (physical enhancement by the mesoporous Au nanostructures and chemical enhancement by HMOF), chemical recognition by HMOF, and a discriminant function for bio-samples containing large biomolecules, such as blood components. We demonstrate the effect of each component (mesoporous Au and microporous AlaZnCl (HMOF)) on the analytical performance for sensing. The growth of AlaZnCl leads to an increase in the SERS signal (by around 17 times), while the use of mesoporous Au leads to an increase in the signal (by up to 40%). In the presence of a complex biomatrix (blood serum or plasma), the hybrid hierarchical porous substrate provides control over the transport of the molecules inside the pores and prevents blood protein infiltration, provoking competition with existing plasmonic materials at the limit of detection and enantioselectivity in the presence of a multicomponent biomatrix.

1. Introduction

Mesoporous materials have attracted considerable attention in recent years. Their excellent performance is a result of a large surface area and abundant catalytic active sites. In particular, crystalized mesoporous metallic materials have many low-coordinated atoms, which are catalytically active and efficiently exposed on concave pore architectures (Iqbal et al., 2020; Kani et al., 2021). To date, various applications, including biomedicine (Wang, 2009), heterogeneous catalysis (Øye et al., 2006), and sensing (Wang et al., 2018), have been reported. Mesoporous materials composed of noble metals are very attractive in current science and technology because they exhibit high electrical conductivity and high chemical stability. Moreover, owing to three-dimensional (3D) intertwined porous structures consisting of rounded tips, mesoporous Au structures have shown high potential for surface-enhanced Raman spectroscopy (SERS) with an enhancement factor varying from 10^5 to 10^7 (Li et al., 2015; Lim et al., 2020b). However, the critical issue that requires attention is the low

* Corresponding author. Research School of Chemistry and Applied Biomedical Sciences, Tomsk Polytechnic University, 634049, Tomsk, Russian Federation.
** Corresponding author. Australian Institute for Bioengineering and Nanotechnology (AIBN), The University of Queensland, Brisbane, QLD, 4072, Australia.
E-mail addresses: guselnikovaoa@tpu.ru, guselnio@vscht.cz (O. Guselnikova), y.yamauchi@uq.edu.au (Y. Yamauchi).

https://doi.org/10.1016/j.bios.2021.113109
Received 27 August 2020; Received in revised form 5 January 2021; Accepted 19 February 2021
Available online 24 February 2021

selectivity/specificity of molecular adsorption in these pores. The introduction of an additional functional layer can further increase the selectivity of specific adsorption in the pores and also provide control over the transport of the target molecules inside the pores, preventing undesired adhesion (Clair and De Oteyza, 2019; Sosa-Vargas et al., 2017).

The above strategy can be beneficial for SERS, where prefiltration by functional pores allows isolation of the target analyte from the complex mixture at the nanoscale level, leading to enhanced sensing selectivity (Innocenzi and Malfatti, 2019; Restaino and White, 2019). To date, plasmonic nanoparticles (NPs), such as spheres, nanorods, multi-branched structures, and films coated with mesoporous silica shells (as a dielectric porous medium), have demonstrated applicability for the sensing of different dyes, such as rhodamine 6G (R6G), rhodamine B, crystal violet, and methylene blue (Gao et al., 2016; Innocenzi and Malfatti, 2019; Lin et al., 2015). Potentially, porous silica-coated NPs can provide a high surface area for analyte entrapping, a high enhancement factor (EF), and control of the hot spot distribution (Innocenzi and Malfatti, 2019). However, such SERS applications with mesoporous materials encounter a few significant obstacles for sensing relevant analytes: (i) the relatively long distance (due to the thick silica shell) from the adsorbed analyte to the plasmonic surface considerably limits the sensitivity; (ii) despite the silica coating, there is a risk of uncontrolled aggregation of the NPs, which limits the reproducibility; and (iii) selection of target molecules is based solely on their size, which leads to insufficient selectivity.

Overcoming these limitations can fulfill the requirements of functional, selective, and sensitive SERS substrates. The aforementioned issues can be solved through the functionalization of the mesoporous Au surface and attachment of an additional functional layer, such as metal organic frameworks (MOFs). MOF films provide nanoporous functionality *via* a periodic network structure formed by metal ions and organic ligands. MOFs have proven their superiority in various applications, including sensing (Bilal et al., 2019; Marpaung et al., 2019; Zhang et al., 2020), where, depending on the nature of the metal species and ligand structures, extremely high selectivity of adsorption can be achieved (Liu et al., 2012; Miliutina et al., 2019). When using chiral ligands, the MOF structure becomes homochiral (HMOFs) and provides an opportunity for enantioselective adsorption of chiral analytes and their chemical recognition (Lu et al., 2019). The potential for modifying mesoporous plasmonic films with functional MOFs has prompted new interest in applying such MOFs for enantioselective SERS sensing.

Here, we propose a new class of hierarchical porous Au films, which consist of mesoporous Au with HMOF grown inside the pores, which is extremely appealing for enantioselective SERS in complex biomatrix media. As a functional layer, the HMOF film is based on the chiral ligand (alanine derivative) and abbreviated as *L/D*-AlaZnCl (Pan et al., 2015) (Fig. 1, S2). Consequently, we report a porous SERS sensor showing high potential for the chiral detection of regulated neurotransmitters, where pseudoephedrine was used as an example (Sun and Zhang, 2020). To demonstrate the advantages of hierarchical porous Au films, we also study the applicability of *L/D*-AlaZnCl for biosensing in blood serum and plasma. We demonstrated the advantages of developed sensing system for the analysis of pseudoephedrine in complex multi-component samples.

2. Results and discussion

2.1. Surface-assisted growth of L/D-AlaZnCl on mesoporous Au

The initial mesoporous Au films were prepared by a soft-templating method using self-assembled micelles of diblock copolymers, polystyrene-*block*-poly(ethylene oxide), and electrochemical deposition (Li et al., 2015). The prepared films (thickness of 150 nm) had uniform mesopores with a mean size of 26.2 nm and a standard deviation of 5 nm (Fig. 2a and S3a,c). The homogeneous distribution of the pores over the entire Au-deposited area of the film is expected to provide interesting plasmonic properties. It has previously been demonstrated that these mesoporous structures exhibit propagating surface plasmon polaritons (SPPs) along with intertwined metal structures and localized surface plasmon resonance (LSPR) within its interconnected porous framework and at the round tips (Rao et al., 2017). To prepare the hierarchical porous film, surface-assisted growth of the nanoporous HMOF AlaZnCl was performed *via* the modification of Au using 4-carboxybenzenediazonium tosylate to allow adsorption of nucleation centers to enable HMOF growth (Fig. 1, S1, S2).

The 4-carboxyphenyl groups were grafted by soaking the mesoporous Au films in a freshly prepared 3 mM solution of the corresponding salt. Diazonium chemistry was used as an attractive alternative to thiol chemistry because covalent Au–C bonds are stronger than Au–S, as the binding energy is higher by 14.2 kJ mol^{-1} than that of the thiol (Guselnikova et al., 2017; Kalachyova et al., 2017). (see SI, Fig. S1). It is known that electron transfer from Au to the diazonium cation leads to the attachment of the 4-carboxyphenyl group on the Au surfaces (Mesnage et al., 2012). (see Fig. S1 and related discussion). The deposited groups serve as linkers for the subsequent surface-assisted nucleation and growth of AlaZnCl (Miliutina et al., 2019), consisting of Zn^{2+} and alanine-containing ligands (Pan et al., 2015). Further, we slightly modified the vapor-assisted conversion (VAC) method of MOF growth (Virmani et al., 2018) and applied it to the deposition of two types of HMOF with opposite chirality (*L*-AlaZnCl and *D*-AlaZnCl) using different enantiomers of the chiral ligand (Fig. S2 and related discussion). We performed VAC growth of HMOF by the deposition of a drop of a mother liquid in the presence of ethanol vapors and heating of the reaction vessel, leading to two types of films: Au-*L*-AlaZnCl and Au-*D*-AlaZnCl.

2.2. Surface characterization of Au-L/D-AlaZnCl

The morphology of the as-prepared Au-*L/D*-AlaZnCl was characterized by scanning electron microscopy (SEM). The SEM image of the top surface (Fig. 2a) of the Au film showed homogeneous mesopores with a diameter of 26.2 nm (Fig. S3a,c). Atomic force microscopy (AFM) also demonstrated surface roughness with a root mean square roughness (Rq) of 6.5 nm (Fig. 2c). After the surface-assisted growth of AlaZnCl, the surface morphology was dramatically changed, and the initial structure was covered by nanoporous HMOF, although it still retained its mesoporous structure (Fig. 2b and S3b). The evaluation of the pore-size distribution showed a decrease in the pore diameter to ~18.2 nm due to the filling of the pores by the HMOF (Fig. S3d). The difference in the diameter of the pores between pristine and modified Au films (Fig. S3b, d) showed that the maximum effective thickness of the AlaZnCl film was 4 nm on each side of the pore walls, which is consistent with the XPS results (Table S1 and related discussion). The attenuation of the Au 4*f* signal after HMOF deposition was used to calculate an average HMOF thickness of 3.3 nm, assuming an XPS spot size of 200 μm^2. In addition, AFM analysis showed the appearance of additional morphological features (with a size of 1.2 nm according to (Kundu et al., 2013)) due to the nanoporous film deposition (Fig. 2c and d), leading to an increase in Rq to 7.3 nm. The changes in the nanoscale features were clearly observed in our high-magnification AFM images (Fig. S4a,b). As additional confirmation of AlaZnCl film growth, we evaluated the blockage of the ferrocyanide/ferricyanide redox probe on the Au surface. The voltammogram measured on the pristine Au grating showed typical reduction and oxidation behavior of a diffusion-controlled redox couple (Fig. S4c). After AlaZnCl growth, the peaks became less pronounced. Moreover, the electrochemically active surface areas (ECSAs) were calculated by CV in an acidic medium using 0.5 M H_2SO_4 (Fig. S4d) (Lim et al., 2020a). The ECSA of the pristine mesoporous Au film was 2.87 cm^2 (per 1 cm^2 of geometrical substrate area), while after the growth of AlaZnCl on the Au surface, the ECSA decreased to 1.69 cm^2/cm^2. The observed suppression of the peak intensity (Fig. S4c) and a decrease in ECSA (Fig. S4d) are

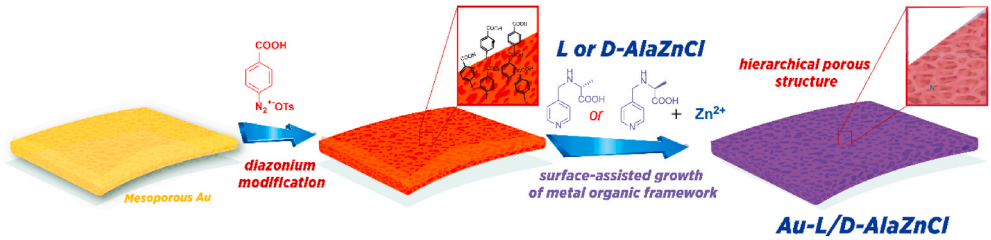

Fig. 1. Schematic diagram showing the preparation of hierarchical porous AlaZnCl-Au films.

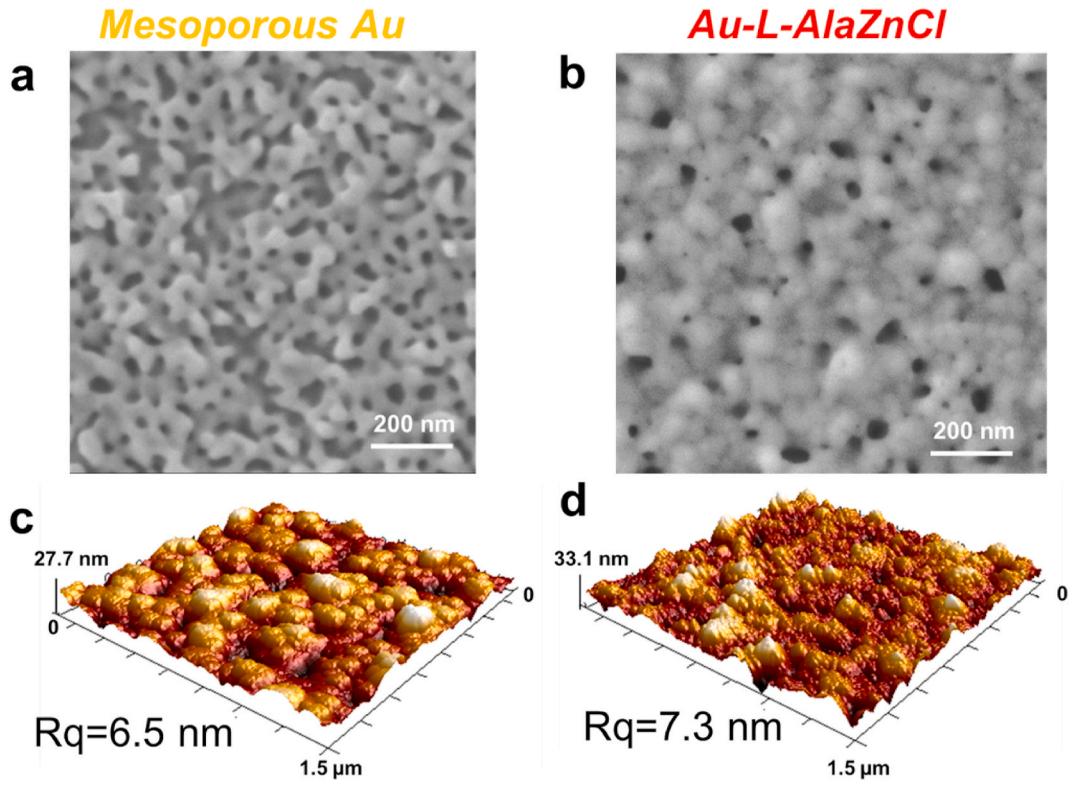

Fig. 2. (a, b) SEM images and (c, d) AFM images of (a, c) mesoporous Au and (b, d) hierarchical porous Au-*L*-AlaZnCl films.

explained by partial surface blocking due to the formation of the AlaZnCl film, while the remaining uncoated Au surface was still electrochemically active owing to the porous structure of the HMOF.

The representative optical reflectance spectra were measured from the mesoporous Au film before and after AlaZnCl deposition (Fig. 3a). The formation of the AlaZnCl layer resulted in the broadening of the plasmon resonance peak and a redshift (from 705 nm to 712 nm) due to the change in the dielectric constant of the medium surrounding the plasmon-active mesoporous Au. The crystallinity of the formed AlaZnCl was investigated by X-ray diffraction (XRD) (Fig. 3c). The XRD peaks at 5.8, 11.6, 17.3, and 18.3° indicate the presence of AlaZnCl film on the surface, confirming the formation of the MOF layer with good crystallinity (i.e., ordered and regular porous structure) (Kundu et al., 2013; Pan et al., 2015) (Fig. 3c). The existence of the main characteristic peaks (5.8, 11.6, 17.3°) in the XRD pattern indicates the formation of a homochiral AlaZnCl crystalline film with a previously reported pore size of 1.2 nm (Kundu et al., 2013; Pan et al., 2015). XPS evidence of AlaZnCl growth is provided by the appearance of characteristic peaks of Zn 2*p* at 1022.8 and 1047.8 eV and N 1s at ~400 eV (Fig. 3b), which is consistent with the formation of Zn-containing MOF (Guselnikova et al., 2019). Additionally, the masking of the Au 4*f* signal with the simultaneous increase of C 1s is due to the coating of Au with the *L*-AlaZnCl film (Table S1).

The as-prepared Au and Au-*L*/*D*-AlaZnCl films were investigated by Raman spectroscopy with an excitation laser wavelength of 785 nm (Fig. S5a and related discussion). Au does not produce any significant Raman signal (Fig. 3d). After diazonium modification, new peaks corresponding to 4-carboxyphenyl groups appeared (Table S2) (Liu et al., 2012). After the deposition of AlaZnCl, the intensity of the spectra was amplified by 2–3 times and sharp peaks corresponding to the AlaZnCl powder were observed (Table S2). The results of the microscopy and spectroscopy studies confirmed the growth of the *L*/*D*-AlaZnCl film on the mesoporous Au film with the formation of hierarchically porous structures.

We performed further SERS measurements to understand the Raman signal enhancement mechanism and quantified the EF of the as-prepared Au film, *L*-AlaZnCl, and Au-*L*-AlaZnCl using the standard Raman probe R6G (see Fig. S5a, b and related discussion). To prevent the preconcentration effect of the porous MOF and the increased surface area after MOF deposition (which can lead to incorrect EF values), we used the drop deposition method to calculate the EF values. We found that mesoporous Au enhances the Raman signal at 1345 cm^{-1} by 0.25×10^7 times compared to Si, corresponding to previously reported results for analogue substrates (Li et al., 2015; Lim et al., 2020b), while AlaZnCl deposition increased EF by approximately one order of magnitude (to 10^8) (Fig. S5b). This increase confirms that the AlaZnCl deposition on a

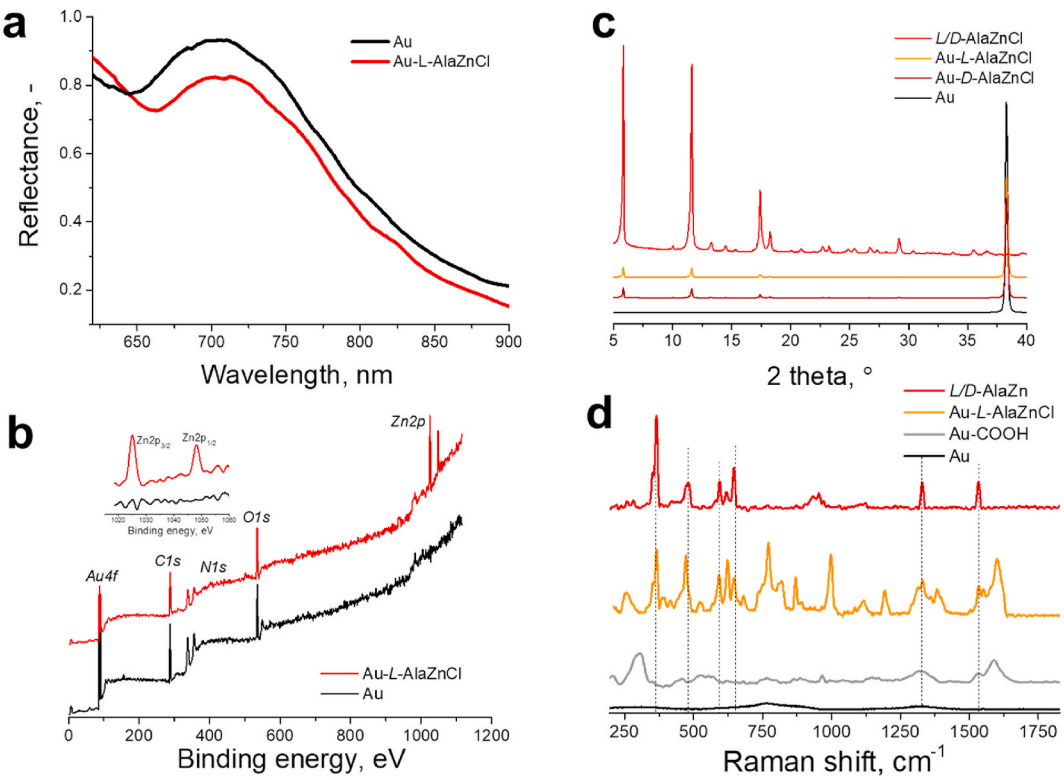

Fig. 3. Characterization of mesoporous Au and hierarchical porous Au-*L*-AlaZnCl films: (a) Optical reflectance spectra, (b) XPS survey (inset: high resolution at Zn 2p peaks), (c) XRD spectra, (d) SERS spectra of Au, Au–COOH, Au-*L*-AlaZnCl, and *L/D*-AlaZnCl (powder).

mesoporous Au film leads to a significant increase in Raman signal intensity and makes the mesoporous Au film with the MOF even more attractive for SERS applications. The additional enhancement is explained by the contribution to SERS through the chemical mechanism provided by the HMOF. The application of MOFs for the enhancement of the SERS signal has been reported recently by various groups (Huang et al., 2020; Lai et al., 2020; Yu et al., 2013). Although the effect is still unclear, it is reasonable to consider charge transfer mechanism based on previous literature(Huang et al., 2020; Lai et al., 2020; Yu et al., 2013). We hypothesized that the enhancement of the signal can be associated with ground-state charge transfer between R6G (or another analyte) and HMOF structural units. The formation of a charge-transfer complex led to a decrease in the highest occupied molecular orbital and lowest unoccupied molecular orbital gap and easier excitation. Chemical enhancement is combined with the physical enhancement of mesoporous Au (electric-field resonance by localized surface plasmon resonance), which results in a high final performance of the designed hybrid structures (Guselnikova et al., 2020).

2.3. SERS activity of Au-L/D-AlaZnCl

The AlaZnCl HMOF has already been shown to selectively capture pseudoephedrine (PE), which is a family of monoamine neurotransmitters (Pan et al., 2016). PE can serve as a drug with one enantiomeric form, in which the presence and conformation need to be strictly monitored (Pan et al, 2015, 2016). Stereoisomeric profiling is of vital importance because different stereoisomers of ephedrine differ significantly in potency, where (−)-pseudoephedrine has much higher stimulant properties than (+)-pseudoephedrine (Rice et al., 2018). Additionally, PE has a high structural similarity to amphetamine and can be a precursor for methamphetamine (Freeman and Alder, 2002), which is restricted in most countries.

Further, we tested the prepared Au-*L/D*-AlaZnCl for the sensing of enantiomers of PE. According to a previous report on (+)-PE (Rice et al., 2018), which is a toxic enantiomer, it can be selectively adsorbed by L-AlaZnCl via molecular recognition mechanism, while (−)-PE enantiomer is dominantly recognized by D-AlaZnCl. To test the enantioselectivity of entrapping by surface-grown HMOF layers (Fig. 4a), we immersed Au-*L*-AlaZnCl in 10^{-6} M enantiopure solutions of both enantiomers for 40 min, followed by SERS measurements (Guselnikova et al., 2020). No spectral difference was detected after immersion in (−)-PE (Fig. S6), while new sharp peaks at 1586, 1292, 972, 810, 680, and 474 cm^{-1} appeared after (+)-PE selective adsorption by Au-*L*-AlaZnCl (Table S3). Therefore, we performed sensing of the model solutions of (+)-PE in the concentration range from 10^{-6} M to 10^{-15} M (Fig. 4b) on Au-*L*-AlaZnCl.

The intensity of the SERS peaks increased with increasing initial PE concentration. The most intense peak at 972 cm^{-1} (C–O stretch and C–H bend vibrations) was chosen to evaluate the relationship between the SERS response and PE concentrations on a logarithmic scale (Fig. 4c). The linear fit shows an excellent relationship with a correlation coefficient of 0.993. Subsequently, we calculated the limit of detection (LOD) of the proposed enantioselective PE discrimination. According to IUPAC recommendations, the minimally acceptable signal intensity must be three times greater than the background signal deviation (*Guideline validation of analytical procedures: text and methodology q2(r1)*, 1995); hence, the LOD could be as low as 10^{-14} M (Fig. 4c). In the case of 10^{-15} M of (+)-PE, the SERS spectrum was very similar to that of Au-*L*-AlaZn and did not provide a pronounced signal (Fig. S7). We also tested *L*-AlaZnCl films to detect (−)-PE; however, the resulting SERS signal at 972 cm^{-1} demonstrated a low intensity (Fig. S6). Therefore, it is evident that Au-*L*-AlaZn is selective towards (+)-PE sensing with ultra-high sensitivity up to femtomolar concentrations. Analogous experiments were performed with Au-*D*-AlaZnCl, and the corresponding concentration dependency is shown in Fig. 4d. The peaks of (−)-PE were registered up to a concentration of 10^{-14} M, while no entrapping of (+)-PE was observed for Au-*D*-AlaZnCl, even at relatively high concentration of 10^{-6} M (Fig. S6). The obtained LOD values for both enantiomers are

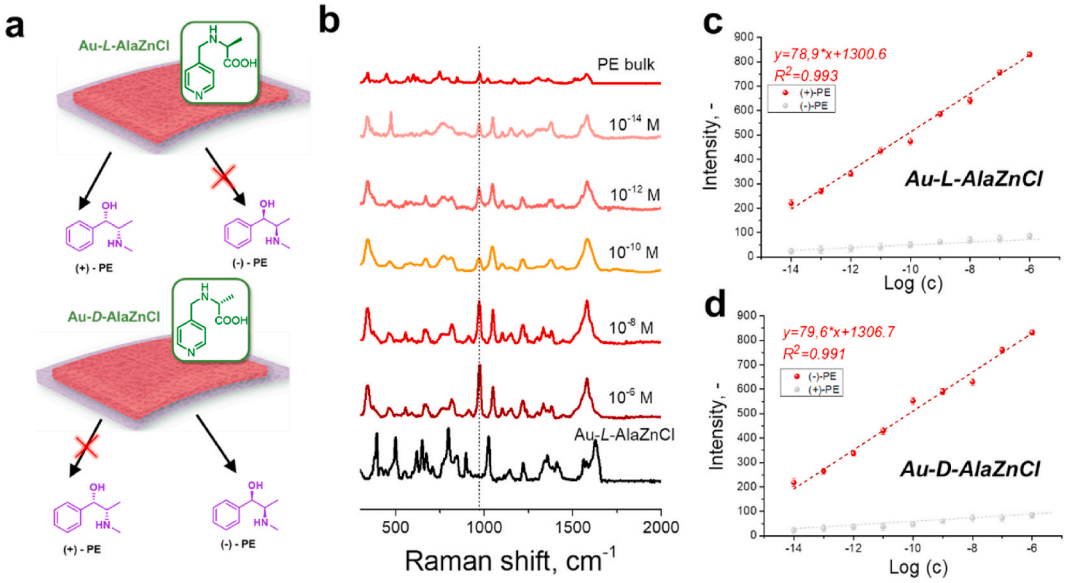

Fig. 4. Characterization of the SERS functionality. (a) Schematic illustrations of enantiomer detections. (b) SERS spectra of Au-*L*-AlaZnCl before and after entrapping (+)-PE (from solutions with various concentrations) and (c, d) the corresponding characteristic PE peak intensity (972 cm^{-1}) as a function of the enantiomers concentrations after their selective entrapping by (c) Au-*L*-AlaZnCl and (d) Au-*D*-AlaZnCl substrates.

extremely low for use as sensing devices for banned substances. The high sensitivity can be explained not only by the dual physical and chemical enhancement but also by selective preconcentration by porous HMOFs.

Moving beyond the detection of a single model analyte, we proved the applicability of the proposed hierarchical plasmonic platform for enantiomer mixture recognition. We tested a mixture containing 10^{-8} and 10^{-6} M of (+) and (−) -PE on both Au-*L*-AlaZnCl and Au-*D*-AlaZnCl substrates. The measured intensity of the SERS peak at 972 cm^{-1} is presented in Table S4 and used as a basis for quantitative estimation of the enantiomeric composition without their preliminary chiral separation (using the calibration curves from Fig. 4c and d). By comparing the real and calculated concentrations, it can be seen that the enantiospecific quantification of the PE concentration is easily achieved within one order of magnitude accuracy even in the presence of the opposite enantiomer.

2.4. Analysis of mixtures with BSA: discriminating the impact of meso- and nanopores

In the analysis of real samples containing neurotransmitters such as PE, the presence of a biomatrix is a major impediment to SERS detection (López-Puente et al., 2013). Furthermore, a number of thiol-containing biomolecules can be strongly adsorbed onto the Au surface, leading to the appearance of additional peaks and making SERS measurements useless. We suggest that the hierarchical structure of Au-*L*/*D*-AlaZnCl in combination with the chiral channels in the MOF structure provides control over the transport of the molecules inside the SERS-active pores (Fig. 5a) and selective chemical recognition of target analytes. Namely, the diffusion of small molecules with high affinity to AlaZnCl into the pores is preferable, while the AlaZnCl film should not entrap macromolecules (molecule size > pore size) from solution. To verify this hypothesis, we compared the analytical performance of Au-*L*-AlaZnCl for (+)-PE (10^{-8} M) mixed with bovine serum albumin (BSA) as a simplified biological medium (Fig. 5b). Without BSA, the spectra of Au-*L*-AlaZnCl show an intensity of 668 of the characteristic peak of (+)-PE with a high signal-to-noise ratio (SNR) of 180.5 (*entry 1*). Analysis of the (+)-PE/BSA mixture showed a slight decrease in peak intensity to 652 and SNR (*entry 2*) in comparison with *entry 1*. However, we observed no new major peaks (Fig. S8), such as those that could arise due to BSA adsorption (Table S5), which confirmed the discriminating function of

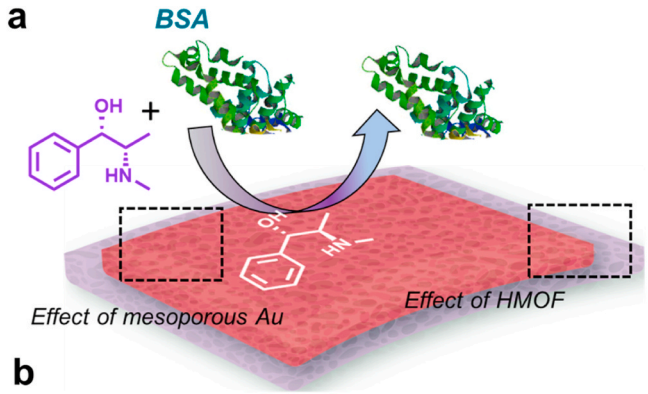

Entry	Substrate	(+) PE, 10^{-8} M	BSA	Intensity of (+) PE,-	Change of intensity, %	SNR
1	Au-*L*-AlaZnCl	+	-	668	+2.5%	180.5
2	Au-*L*-AlaZnCl	+	+	652		163
3	Au	+	+	39	-94%	61.7
4	Au grating	+	+	21	-96.8%	20.2
5	Au grating-*L*-AlaZnCl	+	+	410	-38.6%	60.4
6	Au-*L*-AlaZnCl	+	Human serum	645	-1.2%	160

Fig. 5. (a) Proposed scheme of the filtering action of the surface hierarchical Au-AlaZnCl film and non-porous grating and the (b) corresponding effect of the AlaZnCl and porous Au film on SERS.

the surface.

To obtain the observed preselection phenomena, we compared the analytical performance of the pristine mesoporous Au without an AlaZnCl layer and a non-porous Au plasmonic grating with and without coating by nanoporous AlaZnCl. The results of these experiments provide the contribution of each part of Au-*L*/*D*-AlaZnCl to the analytical performance.

In the case of analysis of (+)-PE/BSA using mesoporous Au without an additional MOF layer (entry 3 in Fig. 5b), the resulting SERS spectra

demonstrated a suppressed peak intensity of (+)-PE (at 972 cm^{-1}) to 94% (or 17 times less consistent with EF calculations)- with reference value *entry 2*, while the major characteristic peaks broadened due to the appearance of BSA-related peaks. Moreover, the SNR of *entry 3* decreased to 61.7 compared with 163 (*entry 2*). To evaluate the contribution of mesoporous Au to the analytical performance of Au-*L/D*-AlaZnCl, we compared the observed SERS response with the response from plasmon-active Au grating (*entry 4*). These Au gratings are similar to mesoporous Au with an EF value of 0.9×10^6 (basic characterization is shown in Fig. S9). The analysis of (+)-PE/BSA demonstrated SERS spectra with a large number of peaks (Fig. S9), most of them masking characteristic PE peaks, making PE detection almost impossible because of the lowest SNR value of 20.2. The growth of AlaZnCl on the Au grating (*entry 5*) led to the sharpest SERS spectrum (Fig. S10) with SNR = 60.4; however, the intensity of the peak at 972 cm^{-1} decreased by 38.6% compared to Au-*L*-AlaZnCl (*entry 5*). The comparison of the analytical performance of plasmonic substrates without nanoporous AlaZnCl and without mesoporous Au clearly confirmed the contribution of each component. The removal of AlaZnCl resulted in a strong suppression of SERS (by 17 times), while the substitution of mesoporous Au resulted in signal suppression up to 40% (e*ntries 3 and 5)*.

2.5. Determination of (+)-PE in human serum and blood plasma: possibilities and limitation of application for real biosensing

Despite the outstanding results obtained for chiral sensing of (+)-PE, the applicability of the sensor strictly depends on selective recognition in biorelevant media. PE is commonly quantified in blood, plasma, or urine to monitor any possible performance-enhancing use by athletes, confirm a diagnosis of poisoning, or assist in a medicolegal death investigation (Kim et al., 2011; Mirmahdieh et al., 2012). Therefore, we tested the applicability of Au-*L*-AlaZnCl for the determination of (+)-PE in the blood plasma and serum, which are biofluids commonly used in diagnostics as an example of a complex biological matrix.

In general, the poor sensitivity during blood analysis is due to signal interference from the blood components, and their strong interactions with noble metallic surfaces block plasmonic spots. Hence, lowering the nonspecific interactions and sorption of proteins, enzymes, hormones, and other blood components (Bonifacio et al., 2014) with metallic surfaces results in an increase in the SERS-substrate sensitivity. We hypothesized that the hierarchical structure of the Au-*L*-AlaZnCl sensor can prevent these unspecific interactions as its surface has size- and chemical-specificity to PE, resulting in a reliable signal even in the complex biomatrix.

First, we tested the interaction of human serum components with Au and Au-*L*-AlaZnCl to estimate the possible interference with the analyte signal. 20 μL of human serum was drop-deposited onto Au and Au-*L*-AlaZnCl surfaces and incubated for 30 min at 3 °C. For the pristine Au, the SERS spectra are characteristic of that of a serum dominated by protein bands, where the peaks at 761, 905, 1320, 1490, and 1650 cm^{-1} were attributed to tyrosine, C–H deformational vibrations, tryptophan, CH_2 deformational vibrations, and β-helix in amide I, respectively (Kim et al., 2011; Li et al., 2013) (Fig. S11). However, no additional significant peaks appeared after incubation on AlaZnCl-coated Au. To examine the applicability of the complex biomixture analysis, we used Au-*L*-AlaZnCl for the sensing of (+)-PE in the human serum matrix. After incubation of Au-*L*-AlaZnCl with the 10^{-8} M solution of (+)-PE in serum and subsequent washing with water and methanol, the resulting SERS spectra were almost identical to those shown in Fig. S8, confirming the functionality of the hierarchical structure (*entry 6*). The intensity of the peak at 972 cm^{-1} decreased to 1.2% with the conservation of the SNR value. These results sufficiently verified the performance to justify further testing with more complex biomatrices.

Undiluted blood plasma was used to prepare the next samples, representing a potentially greater sensitivity challenge for SERS (Phung et al., 2018; Sun et al., 2016). In contrast to serum, plasma contains a number of much larger biomolecules such as globulin (approximately $27.4 \times 16.6 \times 6.3$ nm) and/or fibrinogen (approximately $25.3 \times 6.5 \times 53.5$ nm) (Kenry et al., 2017) that can impede separation by the porous surface of Au-*L/D*-AlaZnCl and block plasmon-active sites (Li et al., 2013; Phung et al., 2018; Sun et al., 2016). Another potential obstacle to efficient biosensing of PE is the presence of other drugs (Caraballo et al., 1995; Lou et al., 2010). Therefore, we tested solutions of PE in citrated undiluted blood plasma in the presence of vancomycin (VN) (Fig. 6a). The composition of the analyzed samples was 10^{-6} M VN in undiluted blood plasma and different amounts of (+)-PE from 10^{-6} to 10^{-12} M. Twenty microliters of the prepared suspensions were deposited on Au-*L*-AlaZnCl and analyzed by SERS. In the case of 10^{-6} to 10^{-10} M concentrations, the spectra did not show any peaks additional to those previously observed for PE (Fig. 6a). The most intense peak at 972 cm^{-1} was used for quantitative analysis according to the linear relation in Fig. 4c, and the obtained results accurately matched the values of the calibration curve and the experimentally added amount of (+)-PE.

In the case of decreasing the concentration of (+)-PE to 10^{-12} M, the peak at 972 cm^{-1} was still well distinguished and was quantified with a value of $10^{-12.4}$ M (LOD), while additional wide peaks appeared at 1320, 905, and 761 cm^{-1}, which were attributed to competitive adsorption of plasma proteins (Li et al., 2013). The comparison of the resulting spectra with the Raman spectra of VN measured on Si wafers (Fig. S12) verifies the conclusion that the peaks are not related to the capturing of VN by MOF structures, but due to the considerable adsorption of blood plasma components. The qualitative analysis of PE at a concentration of 10^{-14} M was already beyond the LOD, evidenced by the calculated concentration being a few orders of magnitude lower than the experimentally added concentration (Fig. S13). Therefore, we defined the LOD of (+)-PE detection in undiluted blood plasma as 10^{-12} M, which is considered to be an excellent sensitivity in the presence of an additional drug.

Further evaluation of the reproducibility of the developed sensor revealed that the analysis of (+)-PE in the concentration range of 10^{-6} to 10^{-12} demonstrated that the relative standard deviation (RSD) of the SERS signal was 2.2% (for 10^{-6} M), 4.9% (for 10^{-8} M), 5.4% (for 10^{-10} M), and 8.4% (for 10^{-12} M). RSD values lower than 10% are considered to be highly reproducible measurements in biosensing and forensic applications (Muehlethaler et al., 2016). High reproducibility was observed, even in the case of extremely low picomolar concentrations, along with high sensitivity. The RSD values are sufficient for analytical analysis (Fan et al., 2020) within one order of magnitude and comparable to chromatographical methods (Odovic et al., 2017; Sardela et al., 2011).

For cross-validation of SERS sensor, the prepared samples were analyzed by gas chromatography (GC) according to (Odovic et al., 2017) (Fig. S14, S15 - calibration curve, and chromatogram, respectively). It should be noted that for the GC analysis, the additional step of pH adjustment and extraction by ethyl acetate (Odovic et al., 2017; Sardela et al., 2011) (and often derivatization) is commonly required, in contrast to the fast single-step SERS measurements. The excellent agreement of SERS-derived data with the GC results, as shown in Fig. 6b (except for picomolar concentrations close to the quantification limit of GC (Evans and Kasprzyk-Hordern, 2014)) within the range of one order of magnitude proves the applicability of hierarchical porous chiral SERS substrates for biosensing. Therefore, SERS sensing using Au-*L*-AlaZnCl can determine PE at concentration one order of magnitude lower than CG, achieving picomolar resolution even in the presence of large biomolecules and other drugs.

To demonstrate the power of the dual-enhancing properties of mesoporous Au and nanoporous AlaZnCl, we prepared a multicomponent mixture containing 10^{-10} M (+)-PE in undiluted blood serum in the presence of an opposite PE enantiomer and two other drugs (VN and omeprazole), which could penetrate the MOF pores. After pretreatment and extraction, the GC results of this mixture were unclear, and the peaks could not be assigned with certainty (Fig. S15b); hence, the

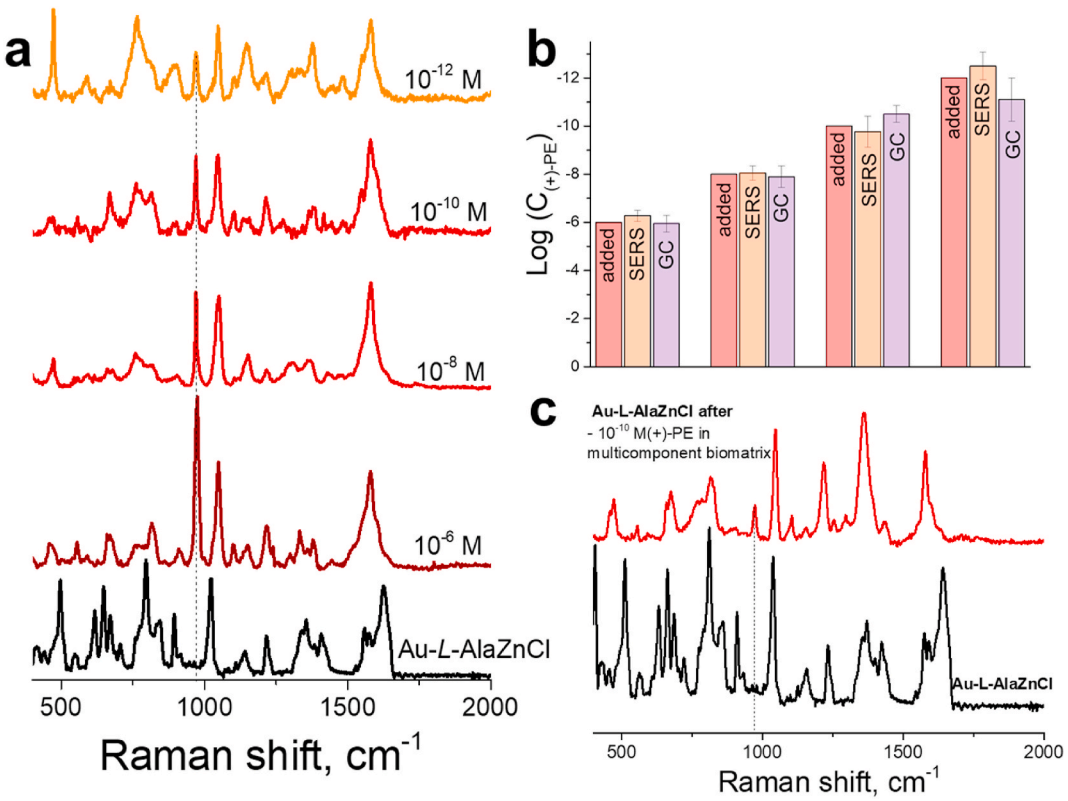

Fig. 6. Applicability of Au-*L*-AlaZnCl for the sensing of (+)-PE in complex biomatrices. (a) SERS spectra from (+)-PE peak detection in the presence of blood plasma after their selective entrapping by Au-*L*-AlaZnCl and subsequent SERS measurements. (b) Results of control measurements comparing the sensing of (+)-PE in blood plasma, measured by our SERS approach and GC. (c) SERS spectra obtained from the sensing of 10^{-10} M (+)-PE in a complex biomatrix (blood serum, 10^{-6} M (−)-PE, 10^{-6} M VN, 10^{-6} M OM).

concentration of (+)-PE could not be estimated. In contrast to GC, the resulting SERS spectra showed a clearly distinguishable peak at 972 cm^{-1} (Fig. 6c), with an intensity corresponding to $10^{-10.3}$ M. This confirms the applicability of the proposed SERS sensor for multicomponent biosamples with high enantioselectivity and sensitivity.

2.6. Reproducibility of sensing with a complex biomatrix

As previously noted, the presence of large biomolecules is likely to affect the sensitivity and reproducibility of SERS sensing due to possible blocking of the Au surface. The reproducibility of SERS signals is an extremely important feature of the SERS biosensing strategy. Therefore, after the quantitative analysis of PE in the presence of blood plasma, we studied the reproducibility of (+)-PE (10^{-8} M) sensing over the film surface. Au-*L*-AlaZnCl was incubated with 10^{-8} M (+)-PE and 10^{-6} M VN, and SERS spectra were collected. The homogeneity of (+)-PE capture by Au-*L*-AlaZnCl was verified by SERS mapping. Fig. 7a shows a SERS map of the intensity of the 972 cm^{-1} peak over an area of the sample of 1.0 × 1.0 mm^2, while b shows the corresponding SERS spectra from the labeled map points. The obtained map showed quite homogeneous distribution of the peak intensity over the area of interest. The RSD of the Raman signals calculated from the SERS map was 4.9%. Moreover, the reliability of the SERS biosensor was evaluated via SERS spectra collection from five different substrates; ten spectra were collected from each substrate to compare the mean signal intensity (at 972 cm^{-1}). As shown in Fig. 7c, the RSD of these values was 3.3%, which indicates good reproducibility and applicability for quantitative analysis (Fan et al., 2020).

Previously reported analogue porous plasmonic systems mostly focused on the sensing of model analytes (dyes, phenanthroline, and thiols) not enantioselective sensing in the presence of large molecules, which is quite different from the actual requirements for bio- or environment-sensing of relevant analytes, (López-Puente et al, 2013, 2015; Yue et al., 2018). These sensors mostly operate via size-exclusion separation, leading to 10^{-7} M level sensitivity without use of a chemical recognition mechanism. The exceptional SERS performance of Au-*L*/*D*-AlaZnCl can be explained by the high Raman signal enhancement derived from mesoporous Au, in addition to the critical role played by AlaZnCl. First, the AlaZnCl film increases the sensitivity by a chemical enhancement mechanism (Fig. 5a). Second, chemical recognition is determined by the internal chiral-recognition environment of AlaZnCl pores (channels or cavities), provided by the chiral architecture, ligand structures, and the metals (Guselnikova et al., 2020; Pan et al., 2015). Third, compared to the pore size of AlaZnCl (≈1.2 nm) (Kundu et al., 2013; Pan et al., 2015), the diameter of PE (≈1 nm) is smaller; thus, PE might enter and move around the chiral channels, while large molecules such as BSA (≈ 280 nm) or other blood components cannot. Au-*L*/*D*-AlaZnCl is an analytical system that has demonstrated excellent performance using complex biosamples with multiple analytes approaching the real application. We demonstrated that the combination of the mesoporous Au structure and additional chiral functionality of grafted AlaZnCl leads to excellent analytical sensing performance for the precise and selective detection of PE from the list of banned drugs and similar relevant compounds.

3. Conclusion

By combining the advantageous behavior of mesoporous Au film and a nanoporous HMOF, we designed and demonstrated a novel family of plasmonic materials to monitor enantiomers of monoamine neurotransmitters. Our novel plasmonic substrates are able to detect and distinguish two PE enantiomers with high enantioselectivity and

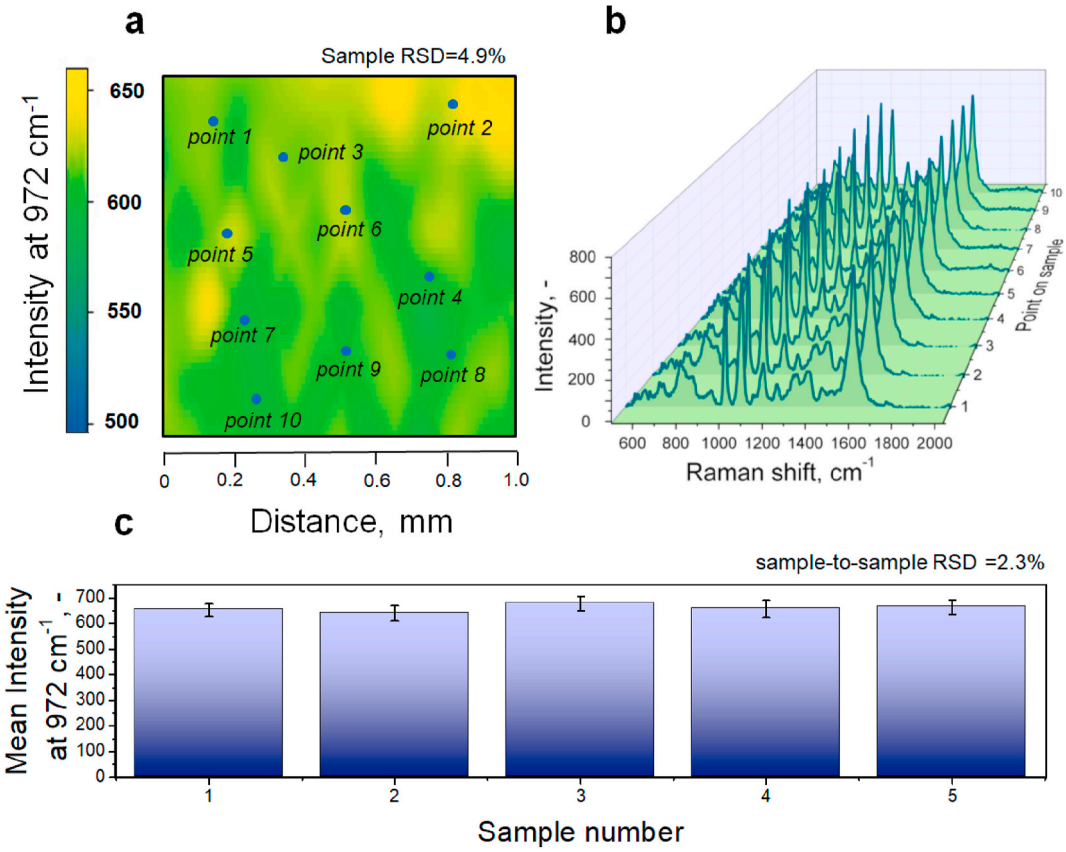

Fig. 7. Reproducibility of (+)-PE (10^{-8} M) sensing in the presence of blood plasma after their selective entrapping by Au-*L*-AlaZnCl (a) SERS map of the 972 cm^{-1} peak intensity. (b) SERS spectra corresponding to the map points. (c) Variations in the peak intensity (calculated as an average value from 10 random measurements) measured on five Au-*L*-AlaZnCl samples.

sensitivity (LOD ~10^{-12} M) in the presence of a complex biomatrix, including their mixtures without preliminary separation. The plasmonic substrates provide dual physical and chemical enhancement of the Raman signal. AlaZnCl provides chemical recognition and a discriminant function for biosamples containing large biomolecules, such as blood serum or plasma components. The synergistic behavior of the hybrid substrates resulted in a smaller LOD and higher enantioselectivity than existing analogues of plasmonic materials. Among other advantages, no sensitivity loss for PE was observed during the analysis of complex biosystems, including an undiluted blood serum mixture with a second enantiomer and the addition of two other drugs. Moreover, in contrast to the most common GC method for PE detection, our SERS sensor does not require an additional pretreatment step before analysis. The PE sensing was reproducible with a signal deviation over a single sample or between samples of < 5%. We envision the potential applications of this general approach not only for SERS applications but also for the design of hierarchical porous platforms for other analytical devices and heterogeneous plasmonic catalysis.

CRediT authorship contribution statement

Olga Guselnikova: Project administration, Visualization, Writing – original draft, Methodology, Conceptualization. **Hyunsoo Lim:** Writing – review & editing, Investigation, Methodology. **Jongbeom Na:** Writing – review & editing. **Miharu Eguchi:** Visualization. **Hyun-Jong Kim:** Investigation. **Roman Elashnikov:** Investigation. **Pavel Postnikov:** Writing – review & editing, Conceptualization. **Vaclav Svorcik:** Funding acquisition, Resources. **Oleg Semyonov:** Investigation. **Elena Miliutina:** Visualization, Investigation. **Oleksiy Lyutakov:** Funding acquisition, Resources, Conceptualization, Writing – review & editing. **Yusuke Yamauchi:** Project administration, Supervision, Methodology, Conceptualization.

Declaration of competing interest

The authors declare that they have no known competing financial interests or personal relationships that could have appeared to influence the work reported in this paper.

Acknowledgements

This research was supported by Tomsk Polytechnic University (Competitiveness Enhancement Program) and Korea Institute of Industrial Technology (KITECH).

Appendix A. Supplementary data

Supplementary data to this article can be found online at https://doi.org/10.1016/j.bios.2021.113109.

Experimental section

Materials and preparation

Materials: (1S,2S)-(+)-Pseudoephedrine, (1R,2R)-(−)-Pseudoephedrine were purchased from Sigma Aldrich. 4-carboxybenzenediazonium tosylate (ADT-COOH) was prepared according to a published procedure (Y. Kalachyova et al., 2017). The ligand N-(4-pyridylmethyl)-l-alanine·HCl (l-HL) was synthesized according to (Pan et al., 2015). Au gratings were prepared according to (Guselnikova et al., 2020). Human serum (from human male AB plasma, USA origin, sterile-filtered, Sigma product number H4522) and human plasma (Citrated plasma, Sigma product number P9523) were used.

Preparation of Au mesoporous films: Au mesoporous films were prepared according to our previous report (Li et al., 2015). Briefly, 10 mg of polystyrene-*b*-poly(ethylene oxide) (PS-*b*-PEO) was dissolved in 3 mL of THF completely at 40 °C, followed by the addition of 1.5 mL of ethanol to the solution. An aqueous solution of $HAuCl_4$ (the final concentration was 5 mM in 8 mL of electrolyte) was added slowly to the clear PS-*b*-PEO solution, and spherical micelles were formed in the presence of water and THF, which are hydrophilic and hydrophobic, respectively. Electrochemical deposition from the precursor solutions was performed using electrochemical workstations (CHI 660E and 760E, CH Instruments, USA) with a conventional three-electrode system, including a platinum wire as the counter electrode, Ag/AgCl as the reference electrode, and a conducting substrate as the working electrode. The electrodeposition of Au was performed at a constant potential of −0.5 V (versus Ag/AgCl reference potential) for 1000 s without stirring at room temperature. After Au deposition, the micelles (used as soft-templates) were thoroughly washed with THF solution at 40 °C, followed by drying with N_2 flow.

Diazonium modification: Mesoporous Au films were spontaneously modified by soaking in a freshly prepared 3 mM aqueous solution of ADT-COOH for 40 min. After modification, the Au films were rinsed under sonication sequentially with water, methanol, and acetone for 10 min and finally dried in air.

Preparation of L/*D-AlaZnCl:* $Zn(CH_3COO)_2{\cdot}2H_2O$ (0.022 g, 0.1 mmol) and 1-HL (0.048 g, 0.2 mmol) were dissolved in 5 mL of EtOH. The solution was then transferred into a Teflon-lined autoclave, followed by heating at 80 °C for 24 h. The reaction products were cooled to room temperature, and the solids were collected by centrifugation, washed with MeOH, and dried at 80 °C for 6 h. After centrifugation, the mother liquid was further used for VAC growth of AlaZnCl films.

Surface-assisted growth of L/D-AlaZnCl: For film formation using VAC, a glass bottle (100 mL) with a PBT cap equipped with a Teflon seal was used. The bottom part of the bottle was filled with Raschig-rings (10×10 mm^2) to obtain an elevated flat platform for the substrate. Then, EtOH was added to the bottle. Afterwards, a substrate (0.3×1 cm^2) was placed on the top of the Raschig-rings and fully coated with a drop of fresh MOF mother liquid. The bottle was closed and transferred to a preheated oven at 60 °C for 3 h. Then, the bottle was removed from the oven and allowed to cool for 10 min before the substrate was removed, washed with EtOH, and dried. See the experimental setup in Fig. S2.

Measurement techniques

X-ray photoelectron spectroscopy (XPS) was performed using an Omicron Nanotechnology ESCAProbeP spectrometer with a monochromated Al K Alpha X-ray source operating at 1486.6 eV. The spectra were recorded using an Omicron Nanotechnology ESCAProbeP spectrometer fitted with a monochromated Al K Alpha X-ray source. The pass energy was set at X (eV) and Y as intensity (cps) for the survey and high-resolution spectra. The energy resolution was 0.4 eV for the survey study and 0.1 eV for the high-resolution investigation. The analyzed area was 200 μm^2. The concentrations of elements were calculated in at.% using the sensitivity factors provided by the manufacturer.

SEM images were obtained using a LYRA3 GMU, Tescan, CR setup with a 10 kV accelerating voltage. Before analysis, the samples were coated with 10-nm Pt layer. The surface morphology was characterized using the peak-force AFM technique (Icon, Brücker). AFM scratch tests were performed on Au films, deposited on microscopic glass substrates, by profiling across a scratch, where the values are reported as the means of 20 values obtained for ten scratches on five samples. XRD data were obtained using an XRD-diffractometer PANalytical X'Pert PRO using Cu Kα radiation (1.5406 Å).

Cyclic Voltammetry (CVA) measurements were performed in a solution of 5 mM potassium hexacyanoferrate (II) trihydrate in 0.1 M potassium chloride. ECSA measurements were performed in 0.5 M H_2SO_4. CVA measurements were performed using a Palm Sens 4 device (Palm Instruments, Netherlands) controlled by PSTrace 5.3 software (March 5, 1127 firmware). The samples were used as the working electrode, a Pt wire was used as the counter electrode, and measurements were performed with a Ag/AgCl (3 M KCl) reference electrode.

Raman spectroscopy measurements

SERS spectra were measured using a ProRaman-L Raman spectrometer (with a laser power of 70 mW and an excitation wavelength of 785 nm), and a Thermo Scientific DXR Raman Microscope (with a laser power 30 mW and an excitation wavelength of 632 nm). The spectra were measured 100 times with a 1 s accumulation time for each measurement. The Raman spectra were used for chemical mapping with a surface area of 1.0×1.0 mm^2 with 50×50 points spaced by a gap of 0.02 mm. The same Raman spectrometer (785 nm and 70 mW) was used for mapping. The spectra were recorded at a resolution of 2 cm^{-1} in the 2000-500 cm^{-1} wavenumber range with an exposure time of 100 s for each exposure. To calculate the RSD from the SERS map, Gwyddion software (Statistical Quantities Tool) was used. For the calculation of RSD between samples, five samples of Au-L-AlaZnCl were tested for sensing 10^{-8} M (+)-PE and 10^{-6} M VN in undiluted citrated human blood plasma. Ten spectra were collected from each sample and the average values were used for the RSD calculation.

Calculation of LOD and SNR: The LOD was calculated using the signal-to-noise ratio (SNR), according to the IUPAC recommendations (INTERNATIONAL, n.d). In particular, the minimal concentration at which the signal-to-noise relation is equal to 3 was defined as the LOD. The standard deviation (SD) of the background signal (noise) was calculated from 20 spectra according to relation $SD = \sqrt{\sum \left|\frac{x-\bar{x}}{N}\right|}$, where x is the intensity of the Raman signal at 972 cm^{-1}, $\bar{x}$ is the mean of the intensities, and N is the number of spectra used. Accordingly, we calculated an SD of 3.2.

The SNR was calculated using:

$$SNR = \frac{\bar{S}}{SD}$$

where $\overline{S}$ is the mean average peak height above the background. This SNR was calculated from 20 samples (N = 20) of (+) PE + (BSA).

Gas chromatography measurements

An 8860 Agilent gas chromatograph equipped with flame ionization detector and fitted with an 8200 Autosampler was used for the cross-validation of the SERS results. The analytes were separated using an HP-5 column (30 m × 0.25 mm × 0.25 μm). Helium was used as the carrier gas at a flow rate of 0.7 mL/min. The injection was performed in splitless mode with a volume of 10.0 μL. The injector and interface temperatures were both maintained at 250 °C. The initial column temperature was set at 80 °C and held for 2 min, followed by temperature ramps of 15 °C/min to 230 °C and held for 2 min. The total run time was 12.50 min.

Sample preparation for GC

A stock solution of PE with a concentration of 10^{-2} M was prepared by dissolving 165 mg of PE in 100 mL ethyl acetate. To prepare a calibration curve, aqueous solutions of ephedrine at concentrations of 10^{-4}, 10^{-5}, 10^{-6}, 10^{-7}, 10^{-8}, 10^{-9}, 10^{-10}, 10^{-11}, 10^{-12}, 10^{-13}, and 10^{-14} M were mixed with 100 μL of saturated sodium bicarbonate, pH was adjusted to 9.0 with 1.0 M sodium carbonate and ethyl acetate. The tubes were vortexed for 30 min and centrifuged (3000 rpm) for 3 min. The ethyl acetate was evaporated to 1 mL and analyzed by GC.

0.48 mL of blood plasma +10 μL of 10^{-6} M vancomycin solution +10 μL of PE solution with concentrations 10^{-8}, 10^{-12}, 10^{-14} M, and 20 μL = resulting solution were deposited to Au-L-AlaZnCl samples for 30 min at 3 °C, washed with water, dried, and analyzed by SERS. To the residual solution, 100 μL of saturated sodium bicarbonate was added to adjust the pH to 9.0, with 1.0 M sodium carbonate and 4.0 mL of ethyl acetate in tubes was added. The tubes were vortexed for 30 min and centrifuged (3000 rpm) for 3 min. The ethyl acetate was evaporated to 1 mL and analyzed by GC.

References

Bilal, M., Adeel, M., Rasheed, T., Iqbal, H.M.N., 2019. Multifunctional metal-organic frameworks-based biocatalytic platforms: recent developments and future prospects. J. Mater. Res. Technol. https://doi.org/10.1016/j.jmrt.2018.12.001.

Bonifacio, A., Dalla Marta, S., Spizzo, R., Cervo, S., Steffan, A., Colombatti, A., Sergo, V., 2014. Surface-enhanced Raman spectroscopy of blood plasma and serum using Ag and Au nanoparticles: a systematic study. Anal. Bioanal. Chem. 406, 2355–2365. https://doi.org/10.1007/s00216-014-7622-1.

Caraballo, I., Fernández-Arévalo, M., Holgado, M.A., Alvarez-Fuentes, J., Rabasco, A.M., 1995. Communications simultaneous hplc determination of some drugs commonly used in cold medications: dextromethorphan, dephenhydramine, phenylephrine, phenylpropanolamine and pseudoephedrine. Drug Dev. Ind. Pharm. 21, 605–613. https://doi.org/10.3109/03639049509048126.

Clair, S., De Oteyza, D.G., 2019. Controlling a chemical coupling reaction on a surface: tools and strategies for on-surface synthesis. Chem. Rev. 119, 4717–4776. https://doi.org/10.1021/acs.chemrev.8b00601.

Evans, S.E., Kasprzyk-Hordern, B., 2014. Applications of chiral chromatography coupled with mass spectrometry in the analysis of chiral pharmaceuticals in the environment. Trends Environ. Anal. Chem. 1, e34–e51. https://doi.org/10.1016/j.teac.2013.11.005.

Fan, M., Andrade, G.F.S., Brolo, A.G., 2020. A review on recent advances in the applications of surface-enhanced Raman scattering in analytical chemistry. Anal. Chim. Acta. https://doi.org/10.1016/j.aca.2019.11.049.

Freeman, S., Alder, J.F., 2002. Arylethylamine psychotropic recreational drugs: a chemical perspective. Eur. J. Med. Chem. https://doi.org/10.1016/S0223-5234(02)01382-X.

Gao, Z., Burrows, N.D., Valley, N.A., Schatz, G.C., Murphy, C.J., Haynes, C.L., 2016. In solution SERS sensing using mesoporous silica-coated gold nanorods. Analyst 141, 5088–5095. https://doi.org/10.1039/c6an01159d.

Guselnikova, O., Postnikov, P., Elashnikov, R., Miliutina, E., Svorcik, V., Lyutakov, O., 2019. Metal-organic framework (MOF-5) coated SERS active gold gratings: a platform for the selective detection of organic contaminants in soil. Anal. Chim. Acta 1068, 70–79. https://doi.org/10.1016/j.aca.2019.03.058.

Guselnikova, O., Postnikov, P., Elashnikov, R., Trusova, M., Kalachyova, Y., Libansky, M., Barek, J., Kolska, Z., Švorčík, V., Lyutakov, O., 2017. Surface modification of Au and Ag plasmonic thin films via diazonium chemistry: evaluation of structure and properties. Colloids Surfaces A Physicochem. Eng. Asp. 516, 274–285. https://doi.org/10.1016/J.COLSURFA.2016.12.040.

Guselnikova, O., Postnikov, P., Kolska, Z., Zaruba, K., Kohout, M., Elashnikov, R., Svorcik, V., Lyutakov, O., 2020. Homochiral metal-organic frameworks functionalized SERS substrate for atto-molar enantio-selective detection. Appl. Mater. Today 20, 100666. https://doi.org/10.1016/j.apmt.2020.100666.

Huang, C., Li, A., Chen, X., Wang, T., 2020. Understanding the role of metal-organic frameworks in surface-enhanced Raman scattering application. Small 16, 2004802. https://doi.org/10.1002/smll.202004802.

Innocenzi, P., Malfatti, L., 2019. Mesoporous materials as platforms for surface-enhanced Raman scattering. TrAC Trends Anal. Chem. (Reference Ed.) 114, 233–241. https://doi.org/10.1016/J.TRAC.2019.02.031.

INTERNATIONAL, INTERNATIONAL CONFERENCE ON HARMONISATION OF TECHNICAL REQUIREMENTS FOR REGISTRATION OF PHARMACEUTICALS FOR HUMAN USE ICH HARMONISED TRIPARTITE GUIDELINE VALIDATION OF ANALYTICAL PROCEDURES: TEXT AND METHODOLOGY Q2(R1), n.d.

Iqbal, M., Kim, Y., Saputro, A.G., Shukri, G., Yuliarto, B., Lim, H., Nara, H., Alothman, A. A., Na, J., Bando, Y., Yamauchi, Y., 2020. Tunable concave surface features of mesoporous palladium nanocrystals prepared from supramolecular micellar templates. ACS Appl. Mater. Interfaces 12, 51357–51365. https://doi.org/10.1021/acsami.0c13136.

Kalachyova, Y., Olshtrem, A., Guselnikova, O.A., Postnikov, P.S., Elashnikov, R., Ulbrich, P., Rimpelova, S., Švorčík, V., Lyutakov, O., 2017. Synthesis, characterization, and antimicrobial activity of near-IR photoactive functionalized gold multibranched nanoparticles. ChemistryOpen 6, 254–260. https://doi.org/10.1002/open.201600159.

Kani, K., Lim, H., Whitten, A.E., Wood, K., Yago, A.J.E., Hossain, M.S.A., Henzie, J., Na, J., Yamauchi, Y., 2021. First electrochemical synthesis of mesoporous RhNi alloy films for an alkali-mediated hydrogen evolution reaction. J. Mater. Chem. A 9, 2754–2763. https://doi.org/10.1039/D0TA09348C.

Kenry, Geldert, A., Liu, Y., Loh, K.P., Teck Lim, C., 2017. Nano-bio interactions between carbon nanomaterials and blood plasma proteins: why oxygen functionality matters. NPG Asia Mater. 9 https://doi.org/10.1038/am.2017.129 e422-e422.

Kim, J.K., Jee, J.P., Park, J.S., Kim, H.T., Kim, C.K., 2011. Reverse-phase liquid chromatography with electrospray ionization/mass spectrometry for the quantification of pseudoephedrine in human plasma and application to a bioequivalence study. Arzneimittel-Forschung/Drug Res. 61, 276–281. https://doi.org/10.1055/s-0031-1296199.

Kundu, T., Sahoo, S.C., Saha, S., Banerjee, R., 2013. Salt metathesis in three dimensional metal-organic frameworks (MOFs) with unprecedented hydrolytic regenerability. Chem. Commun. 49, 5262–5264. https://doi.org/10.1039/c3cc41842a.

Lai, H., Li, G., Xu, F., Zhang, Z., 2020. Metal-organic frameworks: opportunities and challenges for surface-enhanced Raman scattering-a review. J. Mater. Chem. C. 8, 2952–2963. https://doi.org/10.1039/d0tc00040j.

Li, C., Dag, Ö., Dao, T.D., Nagao, T., Sakamoto, Y., Kimura, T., Terasaki, O., Yamauchi, Y., 2015. Electrochemical synthesis of mesoporous gold films toward mesospace-stimulated optical properties. Nat. Commun. 6, 1–8. https://doi.org/10.1038/ncomms7608.

Li, M., Cushing, S.K., Zhang, J., Suri, S., Evans, R., Petros, W.P., Gibson, L.F., Ma, D., Liu, Y., Wu, N., 2013. Three-dimensional hierarchical plasmonic nano-architecture enhanced surface-enhanced Raman scattering immunosensor for cancer biomarker detection in blood plasma. ACS Nano 7, 4967–4976. https://doi.org/10.1021/nn4018284.

Lim, H., Kani, K., Henzie, J., Nagaura, T., Nugraha, A.S., Iqbal, M., Ok, Y.S., Hossain, M. S.A., Bando, Y., Wu, K.C.W., Kim, H.J., Rowan, A.E., Na, J., Yamauchi, Y., 2020a. A universal approach for the synthesis of mesoporous gold, palladium and platinum films for applications in electrocatalysis. Nat. Protoc. 15, 2980–3008. https://doi.org/10.1038/s41596-020-0359-8.

Lim, H., Nagaura, T., Kim, M., Kani, K., Kim, J., Bando, Y., Alshehri, S.M., Ahamad, T., You, J., Na, J., Yamauchi, Y., 2020b. Electrochemical preparation system for unique mesoporous hemisphere gold nanoparticles using block copolymer micelles. RSC Adv. 10, 8309–8313. https://doi.org/10.1039/d0ra01072c.

Lin, M., Wang, Y., Sun, X., Wang, W., Chen, L., 2015. "Elastic" property of mesoporous silica shell: for dynamic surface enhanced Raman scattering ability monitoring of growing noble metal nanostructures via a simplified spatially confined growth method. ACS Appl. Mater. Interfaces 7, 7516–7525. https://doi.org/10.1021/acsami.5b01077.

Liu, B., Shekhah, O., Arslan, H.K., Liu, J., Wöll, C., Fischer, R.A., 2012. Enantiopure metal-organic framework thin films: oriented SURMOF growth and enantioselective adsorption. Angew. Chem. Int. Ed. 51, 807–810. https://doi.org/10.1002/anie.201104240.

López-Puente, V., Abalde-Cela, S., Angelomé, P.C., Alvarez-Puebla, R.A., Liz-Marzán, L. M., 2013. Plasmonic mesoporous composites as molecular sieves for SERS detection. J. Phys. Chem. Lett. 4, 2715–2720. https://doi.org/10.1021/jz4014085.

López-Puente, V., Angelomé, P.C., Soler-Illia, G.J.A.A., Liz-Marzán, L.M., 2015. Selective SERS sensing modulated by functionalized mesoporous films. ACS Appl. Mater. Interfaces 7, 25633–25640. https://doi.org/10.1021/acsami.5b10543.

Lou, H. gang, Yuan, H., Ruan, Z. rong, Jiang, B., 2010. Simultaneous determination of paracetamol, pseudoephedrine, dextrophan and chlorpheniramine in human plasma

by liquid chromatography-tandem mass spectrometry. J. Chromatogr. B Anal. Technol. Biomed. Life Sci. 878, 682–688. https://doi.org/10.1016/j.jchromb.2010.01.005.

Lu, Y., Zhang, H., Chan, J.Y., Ou, R., Zhu, H., Forsyth, M., Marijanovic, E.M., Doherty, C. M., Marriott, P.J., Holl, M.M.B., Wang, H., 2019. Homochiral MOF-polymer mixed matrix membranes for efficient separation of chiral molecules. Angew. Chem. Int. Ed. 58, 16928–16935. https://doi.org/10.1002/anie.201910408.

Marpaung, F., Kim, M., Khan, J.H., Konstantinov, K., Yamauchi, Y., Hossain, M.S.A., Na, J., Kim, J., 2019. Metal-organic framework (MOF)-Derived nanoporous carbon materials. Chem. Asian J. 14, 1331–1343. https://doi.org/10.1002/asia.201900026.

Mesnage, A., Lefèvre, X., Jégou, P., Deniau, G., Palacin, S., 2012. Spontaneous grafting of diazonium salts: chemical mechanism on metallic surfaces. Langmuir 28, 11767–11778. https://doi.org/10.1021/la3011103.

Miliutina, E., Guselnikova, O., Chufistova, S., Kolska, Z., Elashnikov, R., Burtsev, V., Postnikov, P., Svorcik, V., Lyutakov, O., 2019. Fast and all-optical hydrogen sensor based on gold-coated optical fiber functionalized with metal-organic framework layer. ACS Sens. 4, 3133–3140. https://doi.org/10.1021/acssensors.9b01074.

Mirmahdieh, S., Khayamian, T., Saraji, M., 2012. Analysis of dextromethorphan and pseudoephedrine in human plasma and urine samples using hollow fiber-based liquid-liquid-liquid microextraction and corona discharge ion mobility spectrometry. Microchim. Acta 176, 471–478. https://doi.org/10.1007/s00604-011-0743-8.

Muehlethaler, C., Leona, M., Lombardi, J.R., 2016. Towards a validation of surface-enhanced Raman scattering (SERS) for use in forensic science: repeatability and reproducibility experiments. Forensic Sci. Int. 268, 1–13. https://doi.org/10.1016/j.forsciint.2016.09.005.

Odovic, J., Markovic, B., Vladimirov, S., Karljikovic-Rajic, K., 2017. Apremilast (otezla) [Internet]. In: CADTH Common Drug Reviews. Oxford Academic. https://doi.org/10.1093/CHROMSCI.

Øye, G., Glomm, W.R., Vrålstad, T., Volden, S., Magnusson, H., Stöcker, M., Sjöblom, J., 2006. Synthesis, functionalisation and characterisation of mesoporous materials and sol-gel glasses for applications in catalysis, adsorption and photonics. Adv. Colloid Interface Sci. 123, 17–32. https://doi.org/10.1016/j.cis.2006.05.010.

Pan, C., Wang, W., Chen, X., 2016. In situ rapid preparation of homochiral metal-organic framework coated column for open tubular capillary electrochromatography. J. Chromatogr. A 1427, 125–133. https://doi.org/10.1016/j.chroma.2015.12.020.

Pan, C., Wang, W., Zhang, H., Xu, L., Chen, X., 2015. In situ synthesis of homochiral metal-organic framework in capillary column for capillary electrochromatography enantioseparation. J. Chromatogr. A 1388, 207–216. https://doi.org/10.1016/j.chroma.2015.02.034.

Phung, V.D., Jung, W.S., Nguyen, T.A., Kim, J.H., Lee, S.W., 2018. Reliable and quantitative SERS detection of dopamine levels in human blood plasma using a plasmonic Au/Ag nanocluster substrate. Nanoscale 10, 22493–22503. https://doi.org/10.1039/c8nr06444j.

Rao, W., Wang, D., Kups, T., Baradács, E., Parditka, B., Erdélyi, Z., Schaaf, P., 2017. Nanoporous gold nanoparticles and Au/Al_2O_3 hybrid nanoparticles with large tunability of plasmonic properties. ACS Appl. Mater. Interfaces 9, 6273–6281. https://doi.org/10.1021/acsami.6b13602.

Restaino, S.M., White, I.M., 2019. A critical review of flexible and porous SERS sensors for analytical chemistry at the point-of-sample. Anal. Chim. Acta 1060, 17–29. https://doi.org/10.1016/j.aca.2018.11.057.

Rice, J., Proctor, K., Lopardo, L., Evans, S., Kasprzyk-Hordern, B., 2018. Stereochemistry of ephedrine and its environmental significance: exposure and effects directed approach. J. Hazard Mater. 348, 39–46. https://doi.org/10.1016/j.jhazmat.2018.01.020.

Sardela, V.F., Sardela, P.D.O., Pereira, H.M.G., Aquino Neto, F.R., 2011. Consequences of the formation of 3,4-dimethyl-5-phenyl-1,3-oxazolidine on the analysis of ephedrines in urine by gas chromatography and a new method for confirmation as N-trifluoroacetyl-O-t-butyldimethylsilyl ether derivatives. J. Chromatogr. A 1218, 1266–1272. https://doi.org/10.1016/j.chroma.2010.12.120.

Sosa-Vargas, L., Kim, E., Attias, A.J., 2017. Beyond "decorative" 2D supramolecular self-assembly: strategies towards functional surfaces for nanotechnology. Mater. Horizons 4, 570–583. https://doi.org/10.1039/c7mh00127d.

Sun, F., Hung, H.C., Sinclair, A., Zhang, P., Bai, T., Galvan, D.D., Jain, P., Li, B., Jiang, S., Yu, Q., 2016. Hierarchical zwitterionic modification of a SERS substrate enables real-time drug monitoring in blood plasma. Nat. Commun. 7, 1–9. https://doi.org/10.1038/ncomms13437.

Sun, Y., Zhang, S., 2020. Application of capillary electrophoresis for ephedrine and pseudoephedrine detection: a review. Int. J. Electrochem. Sci 15, 2614–2623. https://doi.org/10.20964/2020.03.38.

Wang, J., Ma, Q., Wang, Y., Li, Zhiheng, Li, Zhihao, Yuan, Q., 2018. New insights into the structure-performance relationships of mesoporous materials in analytical science. Chem. Soc. Rev. 47, 8766–8803. https://doi.org/10.1039/c8cs00658j.

Virmani, E., Rotter, J.M., Mähringer, A., Zons, T., Godt, A., Bein, T., Wuttke, S., Medina, D.D., 2018. On-surface synthesis of highly oriented thin metal-organic framework films through vapor-assisted conversion. J. Am. Chem. Soc. 140, 4812–4819. https://doi.org/10.1021/jacs.7b08174.

Wang, S., 2009. Ordered mesoporous materials for drug delivery. Microporous Mesoporous Mater. 117, 1–9. https://doi.org/10.1016/j.micromeso.2008.07.002.

Yu, T.-H., Ho, C.-H., Wu, C.-Y., Chien, C.-H., Lin, C.-H., Lee, S., 2013. Metal-organic frameworks: a novel SERS substrate. J. Raman Spectrosc. 44, 1506–1511. https://doi.org/10.1002/jrs.4378.

Yue, S., Sun, X.T., Wang, Y., Zhang, W.S., Xu, Z.R., 2018. Microparticles with size/charge selectivity and pH response for SERS monitoring of 6-thioguanine in blood serum. Sensor. Actuator. B Chem. 273, 1539–1547. https://doi.org/10.1016/j.snb.2018.07.062.

Zhang, S., Yang, Q., Xu, X., Liu, X., Li, Q., Guo, J., Torad, N.L., Alshehri, S.M., Ahamad, T., Hossain, M.S.A., Kaneti, Y.V., Yamauchi, Y., 2020. Assembling well-arranged covalent organic frameworks on MOF-derived graphitic carbon for remarkable formaldehyde sensing. Nanoscale 12, 15611–15619. https://doi.org/10.1039/D0NR03041D.